MAGNETIC COLLOIDAL MICROPUMPS

A Thesis

By

Thomas Charles Henighan

The Ohio State University
2010

Examination Committee:

Dr. Ratnasingham Sooryakumar, Adviser

Dr. Fengyuan Yang

Dedicated to Dr. Soory

INTRODUCTION

The usefulness of microfluidic devices for diverse biological applications such as chemical analysis of blood serum, DNA sequencing, and cell separation have shown superior performance over many current techniques such as flow cytometry [1]. However, widespread adoption of microfluidic technology requires fluid handling devices which are small enough to be integrated into microchannels and ideally such devices should be inexpensive to be disposable. In recent years many non-mechanical pump designs have been proposed which are based on interfacial phenomena such as hydrophilic surfaces [2,3], electrical manipulation of immiscible droplets of KCl in water [4], and electro-osmosis [5]. Unlike their mechanical counterparts, these non-mechanical designs require specific conduit surface chemistries, addition of immiscible liquid to fluid being pumped, and/or that the fluid being pumped be ionic.

The common mechanical micropumps fall into three categories based on the mechanical action used: check-valve [6,7], peristaltic [8], and rotary pumps [9]. They can also be categorized by actuation technique: pneumatic [7,8], piezoelectric [6], or external electric motor [9]. These actuation techniques have been proven for research purposes at microscales, but do not show promise for scaling down to the nano-regime. Moreover, such techniques are generally too expensive to be disposable and require physical attachment to the outside world, whether through pneumatic hoses, wires, or mechanical components. A pump which is comprised of easily obtainable components that can be

scaled down to be used in nanofluidic devices, and which does not require physical attachment to external drives is highly desirable.

Colloidal particles with sizes similar to relevant dimensions of micro and nano fluidic devices are widely available and affordable. Precise manipulation of colloidal micro and nano particles is now realizable thanks to advancements in optical tweezers [10,11], cantilever-tip technologies [12,13], and electrophoresis [14,15]. It has been shown that colloidal micro-particles manipulated via optical tweezers within a microchannel can be used to pump fluid [16]. While optical tweezers present the advantage of eliminating physical attachments to the microfluidic device, the equipment is expensive and the setup sensitive to vibrations.

In this study we utilize localized magnetic field gradients to manipulate colloidal micro-spheres inside microfluidic channels as an actuation technique for mechanical micropumps. Reprogrammable magnetization profiles created through lithographically patterned discrete ferromagnetic disks are utilized as a template for producing highly localized trapping fields. The resulting tunable magnetic field gradients in the vicinity of the disk periphery enable directed forces to be applied on colloidal magnetic micro-particles. By manipulating the particles with these directed forces, the particles can push fluid through microfluidic channels. We present check valve, peristaltic and rotary pump geometries to illustrate the potential of this actuation technique.

METHODS

The experimental layout is illustrated in Fig. 1. Central to the study are the circular permalloy disks (5-10 μm in diameter and 40 nm thick) lithographically patterned on a silicon surface (see Appendix A). The externally applied tuning magnetic fields are provided by two pairs of orthogonal miniature electromagnets to create rotating in-plane fields Hx and H_y, while a circular coil (solenoid) generates the out-of-plane field Hz. Relatively uniform in- and out-of-plane magnetic fields up to 100 Oe are produced with this setup. The electromagnets were each connected to independent current channels programmed in Labview software to produce controlled planar magnetic fields; the direction of Hz was also reversed through programmed routines.

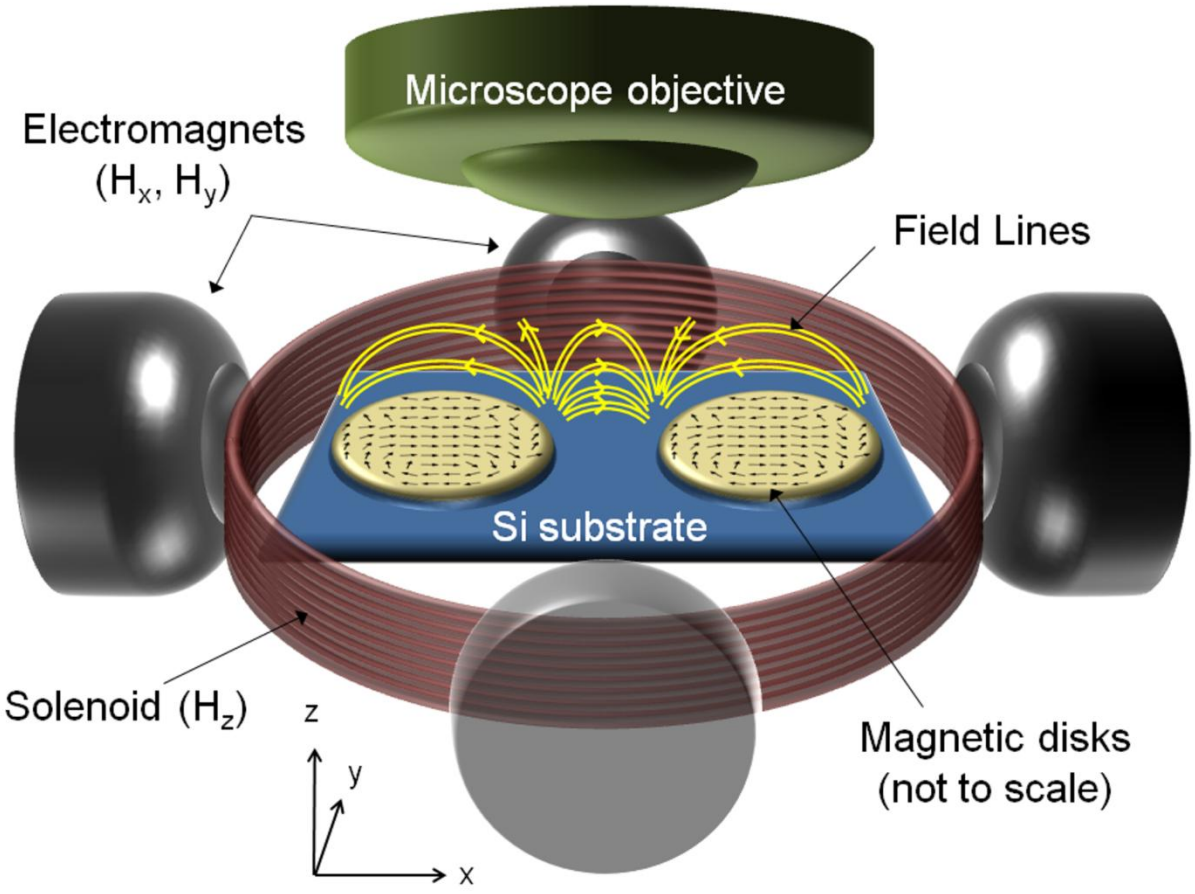

Figure 1: Schematic representation of experimental setup. Circular ferromagnetic permalloy disks are lithographically patterned on a silicon surface. The vectorial maps from OOMMF simulations of the magnetic configurations using a cell size of 50 nm over the 5 μm diameter × 40 nm thick disks in the presence of Hx =50 Oe are shown along with the disks. The magnetization profiles are tuned by four remotely controlled electromagnets that produce rotating in-plane fields Hx, Hy. Reversible perpendicular fields, Hz, are produced by the circular solenoid coil. Movements of cells are recorded by an optical microscope (Leica) with a 10× objective and high speed camera.

SPR-220-7.0 photoresist (Rohm and Haas, Philadelphia, PA) was deposited onto the permalloy disk/silicon substrate and utilized to fabricate the conduit walls as illustrated in figure 2. The best results were achieved by spin-coating the SPR-220 on the substrate at 3000 rpm for one minute then baking at 115^{o}C for 2 minutes. Projection lithography equipment available in the Electronic & Magnetic Nanoscale Composite Multifunctional Materials (ENCOMM) laboratory at The Ohio State University was utilized for exposures and mask fabrication. The best lithography results were achieved by adjusting the light source Olympus TH3 power supply adjustment to "10" (control of light intensity), exposing for 1 minute 15 seconds through the 100x objective of the Olympus BH2-UMA microscope, and soaking in MF-24A developer with gentle agitation for one minute. It was found that when adjusting the focus of the sample and the mask, it is important to focus on the top surface of the photoresist as opposed to the bottom surface where the resist meets the silicon and disks. This process produces a trench in a 10 μm thick layer of photoresist with a floor composed of the silicon wafer and permalloy disks. To contain the fluid from above, a 5 mm thick rectangular sheet of Polydimethylsiloxan (PDMS), a rubbery polymer, was sealed to the top of the structure as illustrated in figure 2(c&f) (Dow Corning Corporation, Midland, Michigan). PDMS does not require an adhesive to bond to the photoresist and can be removed without causing damage. Holes punched into the PDMS created fluid reservoirs which connected to the microchannels.

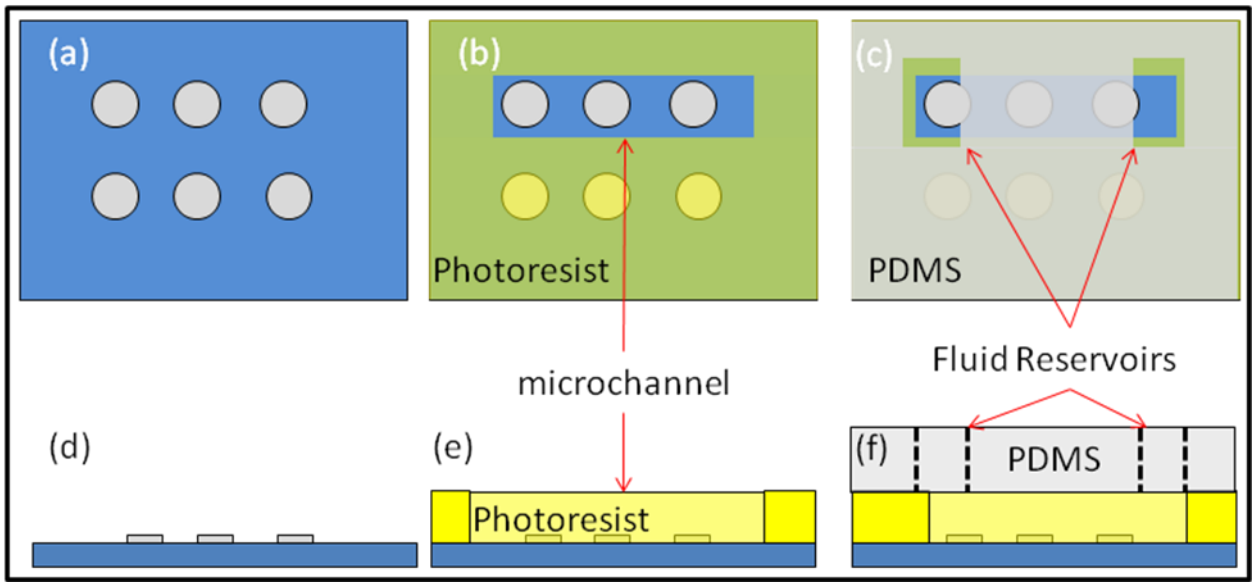

Figure 2: Schematic of silicon substrate with permalloy disks (a&d) with photoresist channel (b&e) and PDMS ceiling with fluid reservoirs (c&f).

Fluid borne polystyrene spheres (diameters of 8.5 and 7.1 µm) embedded with iron-oxide nanoparticles were used to demonstrate the magnetic colloidal particle actuation (Spherotech Inc, Lake Forest IL). These particles are superparamagnetic and their surfaces are coated with a carboxyl group. 2.1 µm diameter polystyrene spheres, also coated with a carboxyl group, were used to track fluid trajectories. The particles were suspended in an aqueous solution which was 0.9% NaCl and 0.4% Pluronic F-68 by weight (BASF corporation, Mount Olive, New Jersey) and 0.05% triton X-100 by volume (Roche Applied Science, Mannheim, Germany).

MODELING

To model the magnetic forces on a microsphere in the lateral and vertical directions we consider magnetization profiles within 5 μm diameter, 40 nm thick permalloy disks. Computer simulations based on the 2D version of object oriented micromagnetic framework (OOMMF) program [17] yielded the micromagnetic structure and its response to the external fields Hx, Hy and Hz. The vectorial maps of the magnetic configurations using a cell size of 50 nm over the permalloy disks (saturation magnetization 8.6×10^5 A/m) in the presence of Hx =50 Oe are illustrated in Fig. 1. The results reveal the magnetization at the disk center to be largely parallel to Hx and curling around the periphery. The vector data from the OOMMF simulation provides for the disk magnetic scalar potential $\Phi_M(\vec{x})$, and field, HDisk (= $\nabla\Phi_M$):

$$\Phi_M(\vec{x}) = -\frac{1}{4\pi}\int_V \frac{\vec{\nabla}'\cdot\vec{M}(\vec{x}')}{|\vec{x}-\vec{x}'|}d^3x' + \frac{1}{4\pi}\oint_S \frac{\hat{n}'\cdot\vec{M}(\vec{x}')da'}{|\vec{x}-\vec{x}'|}. \qquad (1)$$

where $\vec{M}(\vec{x}')$ is the magnetization per unit volume as a function of position derived from the OOMMF simulation and $\hat{n}$ the normal to the disk [18]. The volume integral is performed as a summation over all OOMMF cells. Due to strong shape anisotropy, the magnetization remains largely in plane for the modest out-of-plane fields (Hz < 75 Oe) utilized in this study. When the superparamagnetic particles are in the regime where they are linearly magnetizable, the net magnetic force on the sphere is **F=(½)∇ (m.B)**= (½)$\chi V \nabla B^2 / \mu_o$ where μ_o, V and χ are respectively the free space permeability, volume and linear magnetic susceptibility of the microsphere.

Figs. 2 illustrates the energy, trapping fields and forces associated with a 5 μm diameter × 40 nm thick permalloy disk by external fields Hx**,** Hy as well as their tunability with Hz. Figures 3(a)-(c) show the potential energy profiles for different in plane field directions for Hz = 50 Oe. The sharp potential energy minimum moves along the outer disk periphery tracking synchronously with the direction of the inplane field.

With Hz = 0 (Fig. 2d) two traps A and B are located near diametrically opposite ends parallel to the in-plane field Hx. Figures 3(d) and (e) show that these two traps are approximately symmetric for Hz = 0. The introduction of an axial field Hz (= +50 Oe) directed away from the disk, renders trap B more attractive while weakening trap A (Fig. 2f). Reversing Hz (= -50 Oe) inverts the character of traps A and B (Fig. 2f) that illustrates tunable trapping forces to hundreds of picoNewton.

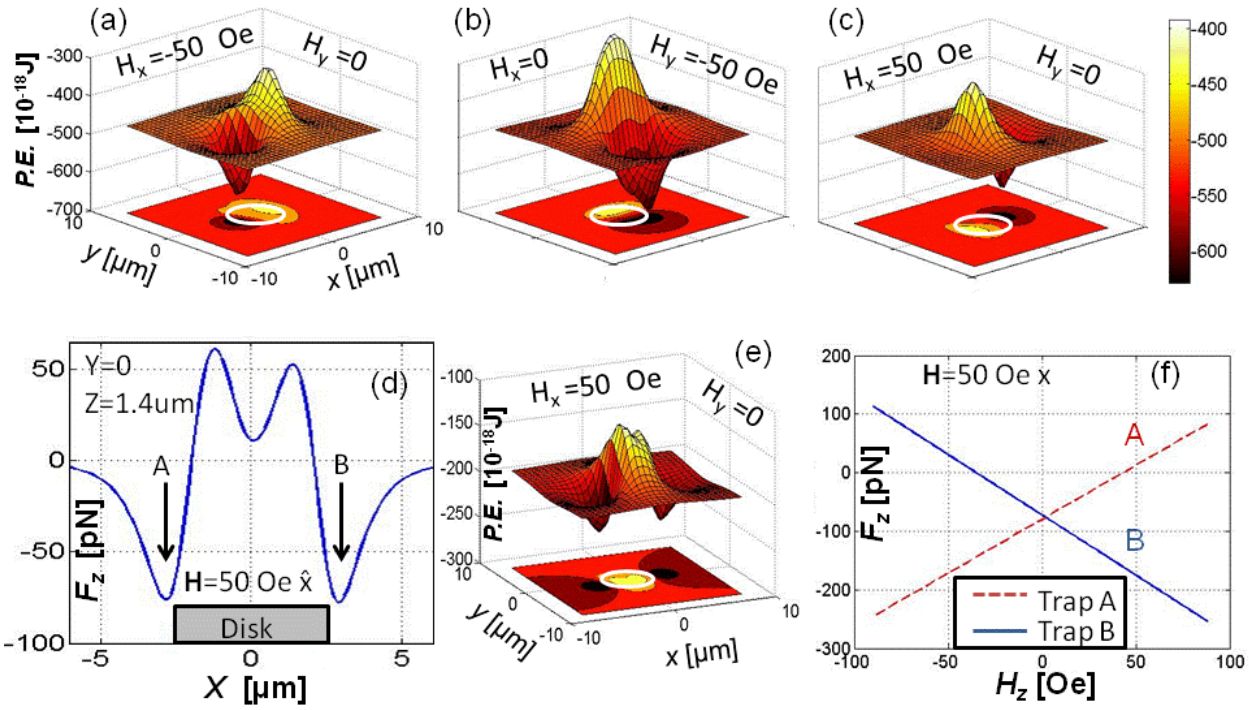

Figure 3: Calculated energy and force profiles from a 5 μm diameter, 40 μm thick permalloy disk magnetized with an in-plane field Hx = 50 Oe. (a)-(c) potential energy (P.E.) profiles of a 2.8 μm magnetic particle (χ=0.85) and contour plot of the energy profile in the x-y plane. With Hz = 0 two traps (A and B) are formed at opposite ends of the disk along the x-axis. The trap strengths are tunable with Hz and its orientation either out of plane (positive) or into plane (negative) determines which trap is enhanced or weakened. (d) F_z, the z-component of the force, on 2.8 μm magnetic particle with Hx = 50 Oe and Hz = 0. The lack of complete symmetry of the energy profile of traps A and B arises from the magnetization of the disk being not perfectly symmetric in the OOMMF simulation. (e) P.E. profile of traps A and B for Hz = 0. (f) The attractive force from Trap A decreases with increasing Hz, with the reverse response for Trap B.

RESULTS

When continuously rotating the direction of H// and keeping Hz constant, the magnetic trap of a thin disk (height 40 nm) will continuously revolve around the periphery of the disk, following the periphery. The behavior exhibited by trapped particles (8.5 μm) in this situation for a given rotation frequency is dependent on the diameter of the permalloy disk. For disks with diameters >~30 μm, an H// field rotation frequency of 1Hz, the particle is pushed out of the trap by viscous drag forces when Hz fixed. Thus if many particles are near the disk, they will execute a peristaltic-like motion as each is periodically pulled in and pushed away from the edge of the disk, as illustrated in figure(4a-d). For smaller disk diameters (<~30 μm) the particles track with the rotating magnetic trap and follow a circular trajectory around the disk as seen in figure(4e-f). The peristaltic and rotary pump designs utilize the large disk (200 μm) regimes and small-disk (10 μm), respectively

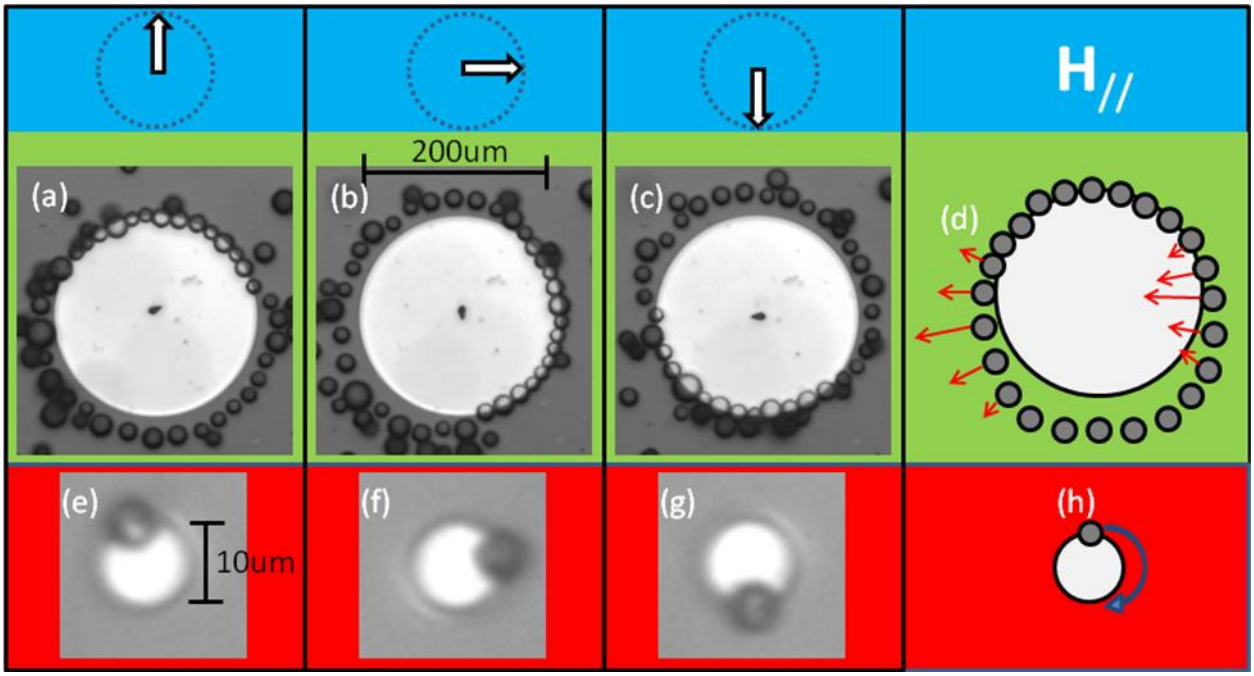

Figure 4: (a-c) Images and (d) schematic of particle behavior for 200 and 10 µm disks under influence of fixed Hz=60 Oe and rotating H//. The white arrows at the top of the figure indicate the direction of H// for that column. For the 200 µm disk, the 8.5 µm magnetic micro-spheres execute a peristaltic motion around the disk as each particle is periodically pulled towards and pushed away from the disk periphery. (e-g) Images and (h) schematic of 10 µm disk. The sphere remains in the magnetic trap and revolves around the disk center, following the periphery.

PERISTALTIC PUMP

To utilize the peristaltic action of the 200 µm disk, we construct a semi-circular channel whose inner wall coincides with the periphery of the disk as illustrated in figure 5a&b. As the external magnetic field is rotated, particles will periodically be pushed into the outer wall and then pulled back into the inner wall to create peristaltic pumping action. The channels extend away from the disk to two fluid reservoirs. To achieve the

configuration of figures 5(b), we add more aqueous micro-particle solution to one reservoir than the other. The solution in the channel will flow in one direction under the influence of the resulting pressure gradient. We then trap 8.5 μm magnetic spheres on the disk as they flow by. Once a suitable number of micro-spheres are trapped, the reservoirs are connected by a larger channel to equalize the pressures.

ROTARY PUMP

For the rotary pump, one magnetic microsphere is used as a paddle as illustrated with the channel geometry shown in figure 5c&d. To capture a sphere on the disk as illustrated in 4(b), the same methodology as mentioned above for the peristaltic pump except that 7.1 μm magnetic spheres were used.

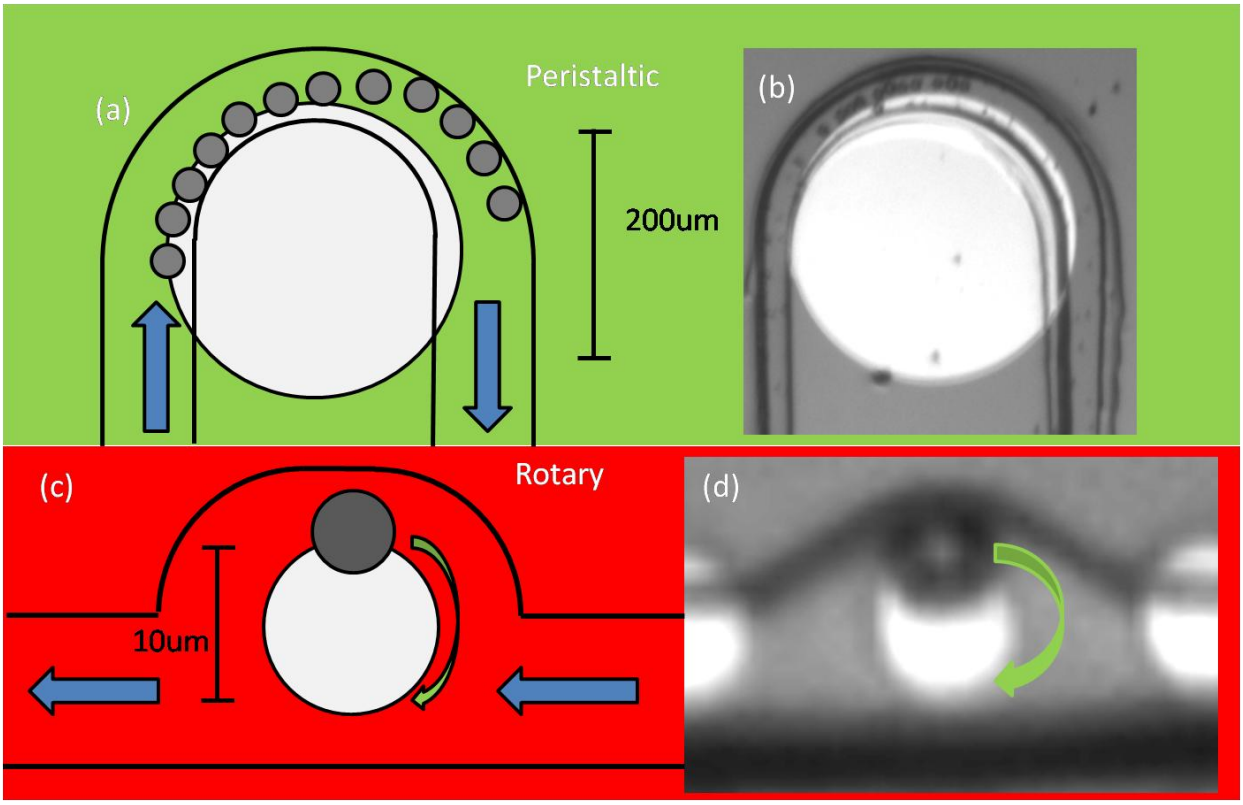

Figure 5: Schematics and Real images of the (a-b) peristaltic and (c-d) rotary micro-pump designs. The disk diameter for the peristaltic pump (a-b) is 200 µm while it is 10 µm for the rotary (c-d). The cannel widths are 20 µm for (b), 10 µm at the thin parts leading away and 20 µm in the center where the disk is for (d) and both are 10 µm deep. The channels lead away from the disks to two fluid reservoirs.

CHECK-VALVE PUMP

Microspheres trapped on the periphery of disks can be repelled away from disk by tuning the external magnetic field Hz so that it opposes the stray fields originating from the disk which are trapping the particle. Hz has negligible effect on the magnetic

structure of the disk due to shape anisotropy, but will affect the magnetization of the superparamagnetic sphere. If the magnitude of Hz is larger than about 50 Gauss, the magnetic moment of the sphere will have a component which points anti-parallel to the trapping fields and the sphere and disk repel one another. If the disks are fabricated in a regular arrangement, the sphere will be repelled away from the first disk to be trapped by the next disk in its path. Repeating the two step process of 1. rotating the direction of H// 180^{o} to transport the particle to the other opposite side of the disk and 2. changing the direction of Hz to repel the sphere to be trapped by the next disk enables transport of the microspheres across the disk array. Because all the disks and spheres are in principle identical, all trapped spheres will move together simultaneously, generating a net flow in the local fluid.

The micropump design illustrated in figure 6 illustrates how the transport of multiple spheres can be used for actuation of a check-valve pump. The larger center chamber houses the disks and particles. By moving the particles downward, fluid is pulled into the chamber from the inlet port (left) while moving them upwards pushes fluid out of the outlet port (right). The Tesla structures incorporated into the input and output ports act as check-valves to ensure a net fluid flow in one direction (left to right here). The Tesla structures promote turbulent flow in one direction (here left to right) and laminar flow in the other (right to left). This results in a greater flow rate in one direction than the opposite direction for a given pressure drop across the Tesla structure. A device which utilizes a pump chamber of straight channels instead of Tesla structures has, in fact,

been fabricated to demonstrate the actuation capability of the microspheres in the pump chamber. While there is no net flow from one straight channel to the other, 2.1 µm spheres in the small branching channels respond to the actuation and their motion shows direct correlation with the motion of the magnetic micro-spheres in the pump chamber. The next step will be to replace the straight channels with Tesla structures to give a preferred fluid flow direction.

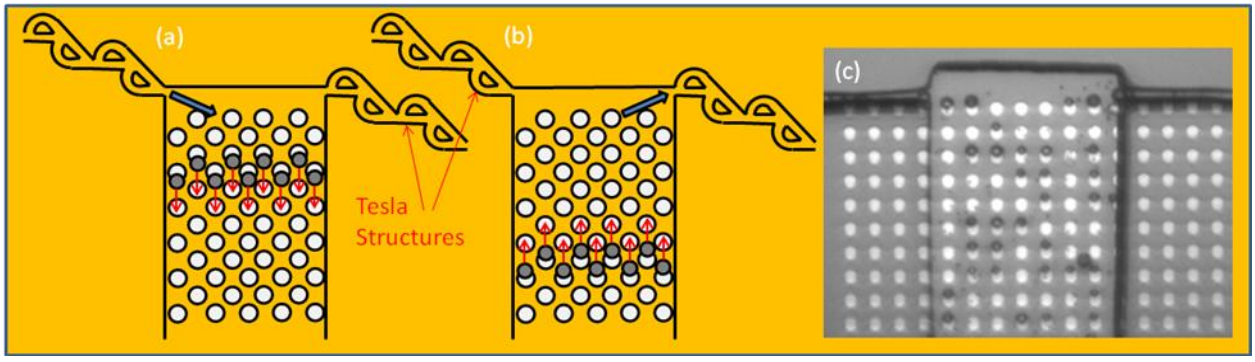

Figure 6: Check-valve pump design. (a) Micro-spheres are transported downwards to generate a net flow in the middle chamber. This pulls fluid from the inlet port (left). The geometry of the inlet port Tesla structure ensures that more fluid will be pulled from the inlet port than the outlet. (b) Micro-spheres are transported upwards to push fluid out of the outlet port (right). (c) Real image of fabricated pump chamber with straight channels instead of Tesla structures. The widths of the larger middle chamber and smaller branching channels are 160 µm and 10 µm respectively. The micro-spheres and disks are 8.5 µm and 10 µm in diameter respectively. Future fabrications of this design will include the disk arrangement shown in (a) and (b) to achieve a higher aerial density of microspheres.

CHALLENGES

Currently, the fluid-pumping capability of these designs has not been measured for the following reasons.

(1). When equalizing pressure in the two reservoirs, the current method of using a pipette to add fluid to each reservoir does not offer precise control of the fluid in the channel. If the fluid speed at the pump becomes too great, viscous forces overcome the magnetic forces and would release the micro-sphere from the magnetic trap. This may be remedied in the future by integrating an external macro-pump to the system (syringe pump) which would allow fine control over flow rates.

(2). It appears that the current method used to equalize the pressure is inadequate since even when the pump is not actuated there is an observed net fluid flow, albeit very small (~2 pL/hr). It is presently unclear if this observed net flow is a result of air bubbles in the channels, a net diffusion of 2.1 μm spheres driven by a concentration gradient, or some other agent.

(3). Triethylene glycol (TEG) cannot be used as a surfactant for the channels as was done in previous work [19, 20] because the photoresist is soluble in ethanol. As a result, adhesion of microspheres to the permalloy commonly renders them immobile. This may be remedied by adjusting the surface chemistry of the device by adding a thin layer of silicon dioxide to the surface with the use of SILICAFILM (Emulsitone Company, Whippany, New Jersey). Published literature suggests that treating this layer in

a UV-ozone cleaner, as is available in the ENCOMM lab, would leave the surface silicon dioxide layer hydrophilic, preventing adhesion [21].

(4). It is very difficult to create channels which are 10 μm thick and 10 μm wide using projection lithography because the incident light strikes the resist at an angle, making it difficult to achieve a 1:1 depth:width aspect ratio. Projection lithography was chosen because it allows for alignment of masks to the disk features with micron-precision and because the equipment is readily available. However, more advanced equipment (mask aligner) available at Nanotech West may provide higher quality microchannels through the use of contact lithography while still achieving high-precision mask alignment.

CONCLUSIONS

Presented here are three designs and early prototypes for a mechanical micropump which is actuated by colloidal magnetic micro-spheres controlled by stray fields of magnetic micro-disks. Advantages of this actuation technique include ease of fabrication, no physical attachments to the device, and the ability to scale to much smaller dimensions. The magnetic field profiles, field gradients, and magnetic forces on microscopic beads have been modeled and calculated. The designs are based on popular micro-pump schemes including peristaltic, rotary, and check-valve pump. Here we have demonstrated the ability to fabricate these devices using lithographic techniques. However, before measurements can be made several problems need to be addressed. These include lack of fluid control, external sources of observed flow, and adhesion.

BIBLIOGRAPHY

1. J.L. DeRisi, V.R. Iyer, and P.O. Brown, "Exploring the Metabolic and Genetic Control of Gene Expression on a Genomic Scale," Science., Vol **278**, 680 (1997).
2. Bin Zhao, *et al.* "Surface-Directed Liquid Flow Inside Microchannels," Science., Vol **291**, 1023 (2001).
3. Dawn E. Kataoka *et al.* "Patterning Liquid Flow on the Microscopic scale," Nature. Vol **402**, 794 (1999).
4. M.G. Pollack, R.B. Fair, and A.D. Shenderov, "Electrowetting-Based Actuation of Liquid Droplets for Microfluidic Applications," Appl. Phys. Lett. Vol **77**, no. 11 (2000).
5. A. Manz, C.S. Effenhauser, N. Durggraf, D.J. Harrison, K. Seiler, and K. Fluri, "Electroosmotic Pumping and Electrophoretic Separations for Miniaturized Chemical Analysis Systems," J. Micromech. Microeng. Vol **4**, 257 (1994).
6. R. L. Bardell "Designing High-Performance Micro-Pumps based No-Moving-Parts Valves," Proc. of Microelectromechanical Systems (MEMS) ASME, Vol **62**, 47 (1997).
7. R. Zengerle and A Richter, "A Micromembrane Pump with Elecrostatic Actuation," Proc. of MEMS'92 5th IEEE International Workshop Micro Electromechanical Systems, Travemunde (Germany) Feb. 4 (1992).
8. M. Unger, H. Chou, T. Thorsen, A. Scherer, S. Quake, "Monolithic Microfabricated Valves and Pumps by Multilayer Soft Lithography," Science. Vol **288**, 113 (2000).
9. J. Dopper, "Micro Gear Pumps for Dosing of Viscous Fluids," Journal of Micromechanics and Microengineering, Vol. **7**, 230 (1997).

10. K.C. Neuman, and A. Nagy, "Single-molecule force spectroscopy: optical tweezers, magnetic tweezers and atomic force microscopy," Nature Methods. Vol **5**491 (2008).
11. D.G Grier, "A revolution in optical manipulation," Nature. Vol **424** 21 (2003).
12. E. Mirowski, J. Moreland, A. Zhang, S.E. Russek and M.J. Donahue, "Manipulation and sorting of magnetic particles by a magnetic force microscope on a microfluidic magnetic trap platform," Appl. Phys. Lett. Vol **86** 2439011 (2005).
13. E. Mirowski, J. Moreland, A. Zhang, S.E. Russek and M.J. Donahue, "Integrated microfluidic isolation platform for magnetic particle manipulation in biological systems," Appl. Phys. Lett. Vol **84** 1786 (2004).
14. M.S. Talary, J.P.H. Burt, J.A. Tame, and R. Pethig, "Electromanipulation and Separation of Cells Using Travelling Electric Fields," Appl. Phys. Lett. Vol **29** 2198 (1996).
15. J. Yang, Y. Huang, X. Wang, F.F. Becker, and P.R.C. Gascoyne, "Cell Separation on Microfabricated Electrodes Using Dielectrophoretic/Gravitational Field-Flow Fractionation," Anal. Chem. Vol **71,** 911 (1999).
16. A. Terray, J. Oakley, and D. W. M. Marr, "Microfluidic Control Using Colloidal Devices," Science, Vol **296**, 1841 (2002).
17. M.J. Donahue, and D. G. Porter 1999 OOMMF User's Guide, Version 1.0, Interagency Report NISTIR 6376, National Institute of Standards and Technology,

Gaithersburg, MD. This public code can be found at the URL http://math.nist.gov/oommf/.

18. Jackson, J.D. 1999. Classical Electrodynamics, 3rd Edition. John Wiley, NY.
19. T. Henighan, G. Vieira, A. Chen, A.J. Hauser, F.Y. Yang, J.J. Chalmers, and R. Sooryakumar, "Manipulation of magnetically labeled and unlabeled cells with mobile magnetic traps". Biophysical Journal. Vol **98**, 412 (2010).
20. G. Vieira, T. Henighan, A. Chen, A. J. Hauser, F. Y. Yang, J. J. Chalmers, and R. Sooryakumar, "Magnetic Wire Traps and Programmable Manipulation of Biological Cells". Phys. Rev. Lett. , Vol **103**, 128101 (2009).
21. D.T. Eddington, J.P. Puccinelli, and D.J. Beebe, "Thermal Aging and Reduced hydrophobic Recovery of Polydimethylsiloxane," Sensors and Acutators B. Vol **114**, 170 (2006).